Measurement Method of High-Frequency Winding Loss in Gapped Inductors Based on Magnetic Field Equivalence

Zhiyong QIU, Kaining FU, and Wei CHEN

***Abstract*—High-permeability cores, such as ferrite, can increase power transfer efficiency and are often designed to be gapped to mitigate magnetic saturation. The fringing effect caused by the air-gap increases the winding loss of the gapped inductor. The key to accurately evaluating its winding loss is extracting that from the total loss. This paper introduces a method for measuring the winding loss of gapped inductors based on magnetic field equivalence. The gapless inductor with the winding for equivalent air-gap was constructed to characterize the magnetic field within the core window of the gapped inductor, and the auxiliary winding was used to replace the winding of the gapped inductor to generate the equivalent magnetizing magnetomotive force. Based on the transformer winding short-circuit method with the small-signal impedance test, the winding loss was separated from the core loss. After the resistance of auxiliary winding was measured by using an air-core inductor, the winding loss of the gapped inductor was consequently obtained. The proposed scheme was applied to inductors made of different sizes and structures, and the measured errors were within 20% in the range of 100 kHz to 1 MHz. The winding loss had a steeper growth tendency in this range than the lower frequency, so the proposed method is effective at high switching frequencies especially.**

***Index Terms*—Fringing effect, gapped inductor, magnetic field equivalence, measurement, winding loss.**

I. Introduction

SWITCH mode power supplies (SMPS) are evolving towards achieving high switching frequency and high power density. Designing magnetic components in power converters has emerged as the paramount challenge impeding further advancements in both efficiency and power density [1]. The losses within magnetic components comprise both winding loss and core loss, which limit the further improvement of the efficiency of power converters.

Winding loss is predominantly influenced by the skin effect, proximity effect, and the impact of fringing flux. High-permeability cores employed in power inductors are typically designed with air-gap to mitigate magnetic saturation [2]. The presence of a gap in the center limb of a magnetic core can give rise to increased eddy current loss, which stem from the fringing effect [3]–[4]. Consequently, numerous investigations have been focused on the winding loss characteristic of gapped magnetic components.

Developing accurate calculation and simulation techniques for winding loss can offer a quantitative evaluation of the winding loss characteristics of gapped magnetic components, which are essential for the optimization of gapped magnetic components.

In [5], T. Ewald presented a theoretically derived computational method for determining the inductance and winding loss of gapped inductors employing both solid-round-wire and Litz-wire configurations, taking into account the influence of fringing flux stemming from the air-gap. However, this method may not be suitable for gapped foil inductors due to the shielding effect of copper foil [6]. The finite element method (FEM) is also a path to solve the winding loss of gapped magnetic components, but it may be impractical for the components using Litz-wire because the numerous strands occupy too much computational resource. Thus, the use of homogenization methods is imperative [7]–[8]. Different from the computational methods such as analytical, numerical, and semi-empirical approaches proposed in previous studies [9]–[11], a semi-analytical model for calculating the winding loss was introduced in [12]. The model combines a concise analytical method with high-precision numerical techniques, significantly enhancing the accuracy of traditional methods.

Currently, the majority of research efforts have been primarily focused on optimizing and theoretically calculating the winding loss of gapped magnetic components. Nevertheless, all of these schemes should be verified by the experimental measurement. So, developing the measurement techniques for

Manuscript received April 22, 2024; revised July 24, 2024; accepted August 18, 2024. Date of publication December 30, 2024; date of current version August 30, 2024. This work was supported by the National Natural Science Foundation of China under Grant 51777036, the Natural Science Foundation of Xiamen Municipality under Grant 3502Z202372043, and the Innovation Project of Xiamen University of Technology under Grant YKJCX2023134. *(Corresponding author: Kaining Fu.)*

Z. Qiu is with the School of Electrical Engineering and Automation, Xiamen University of Technology, Xiamen 361024, China (e-mail: 2222031390@stu.xmut.edu.cn).

K. Fu is with the Xiamen Key Laboratory of Frontier Electric Power Equipment and Intelligent Control, the School of Electrical Engineering and Automation, Xiamen University of Technology, Xiamen 361024, China (e-mail: fkn@xmut.edu.cn).

W. Chen is with the College of Electrical Engineering and Automation, Fuzhou University, Fuzhou 350108, China (e-mail: chw@fzu.edu.cn).

Digital Object Identifier 10.24295/CPSSTPEA.2024.00019

winding loss evaluation in gapped magnetic components is crucial for both theoretical analysis and practical applications. In [13], a measurement method was introduced that aims to capture the winding loss of inductors under the large-signal test. This approach utilizes a reference transformer to offset reactive voltage and the core loss. The winding loss can also be measured by the calorimetric method [14], but it demands stringent requirements for the experimental environment and equipment.

As the relationship between the winding loss and current magnitude exhibits a linear characteristic, a prevalent method for quantifying winding losses is to measure the AC resistance with an impedance analyzer. When assessing the losses in gapped inductors, it is essential to take fully account the impact of the air-gap on the distribution of the magnetic field. Three common misconceptions about the measurement of AC resistance in gapped inductors were summarized in [15], all of which involve the influence of core loss on the measurement results. Hence, when measuring the winding loss of gapped inductors, special attention must be paid to separating the core loss from the measured losses.

The air-gap or other windings can lead to changes in the magnetic field and then cause resistance variations of the measured winding, and this phenomenon is often described as mutual resistance [15]−[17]. For transformers with multiple windings, the winding short-circuit method removes the core loss from the total losses. However, separating the winding loss from the core loss in single-winding inductors can be challenging. Consequently, indirect measurement methods have been developed, involving the construction of auxiliary windings to obtain the core loss of the inductor, which is then subtracted from the total losses [15]−[17]. Due to the influence of high quality factors, the indirect measurement methods can cause large errors in resistance measurement [18]. To solve these problems, [19] proposed a direct measurement scheme. By using a special fixture and employing a three-terminal measurement method, the quality factor can be greatly reduced so that the AC resistance of the winding can be measured directly. However, [17] proved that this method has stringent requirements on the location of the auxiliary winding. A construction method for an effective auxiliary winding was proposed in [17] but the principle of the method was not clearly explained. A method was proposed in [20] to characterize the magnetic field distribution within the core window of the inductor with an air-gap, using a gapless magnetic core and the winding for an equivalent air-gap (WEAG). It is noteworthy that the experimental frequency range in [20] was limited to the range of 10 to 150 kHz and the DC resistance of the Litz-wire was adopted as its AC resistance to remove the winding loss of WEAG. However, as the test frequency rises further, this approach is prone to introduce increasingly significant errors.

In this paper, based on [20], the gapped core of the inductor under test (IUT) was replaced with a gapless core with WEAG. By using the transformer winding short-circuit method, the total AC resistance was obtained, which contains the AC resistance of IUT's winding (R_m) and WEAG (R_s). Subsequently, R_s was measured based on magnetic field equivalence with the help of auxiliary winding, enabling the extraction of R_m. Compared with the existing scheme, the advantage of the proposed scheme is that the auxiliary winding is easy to construct. Due to the balance of ampere-turns between WEAG and IUT's winding, the magnetizing flux inside the core is canceled to lower the quality factor of the inductor. The influence of high quality factors on the measurement result can be reduced. In Section II, the reason why WEAG can be used to replace the air-gap is analyzed in detail. In Section III, the method of how to separate R_m and R_s is exhibited. Section IV experimentally verifies the proposed scheme. Section V presents an error analysis. Finally, Section VI gives the conclusions of this paper.

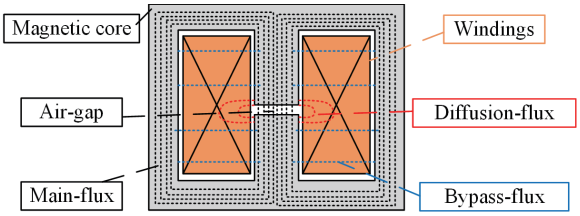

Fig. 1. Distribution of the magnetic field in a gapped inductor with EE-core.

II. Measure the Winding Loss Based on Magnetic Field Equivalence

A. Replace the Air-Gap With Gap Current Sheets

The leakage flux within the window of the inductor's core can induce eddy current loss in the windings, which causes the phenomenon that the AC resistance of the winding exceeds its DC resistance. Fig. 1 shows the distribution of the magnetic field within a gapped inductor with an EE-core. The magnetic fluxes in the inductor are categorized into three types: main-flux, diffusion-flux, and bypass-flux. The main-flux within a magnetic core can cause core loss. Both diffusion-flux and bypass-flux can influence the flux distribution inside the core window, significantly increasing the winding loss of the inductor. Based on this, accurately characterizing the magnetic field distribution within the core window is paramount for precisely evaluating the winding loss of the gapped inductor.

To accurately characterize the magnetic field distribution within the core window of a gapped inductor, a method was proposed in [21] to replace the magnetic potential drop across the air-gap with equivalent ampere-turn current sheets. As depicted in Fig. 2, the gapped core is substituted by a gapless core with "gap current sheets". The gap current sheets are attached to the original location of the air-gap and their heights are equal to the height of the air-gap (δ). When the gap current sheets and the excitation winding reach an ampere-turn balance, the magnetizing ampere-turn by the gap current sheets is then equal to the original magnetic potential drop in the air-gap. This ensures that the magnetic field distribution remains consistent in both configurations.

In order to illustrate the effectiveness of the gap current

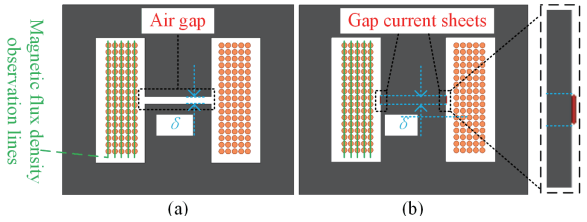

Fig. 2. Inductors with EE-core. (a) Gapped inductor, (b) Inductor with gap current sheets.

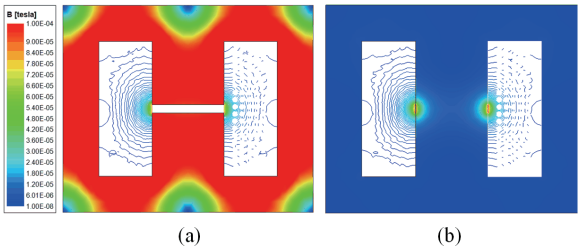

Fig. 3. Magnetic flux density distribution. (a) Gapped inductor, (b) Inductor with gap current sheets.

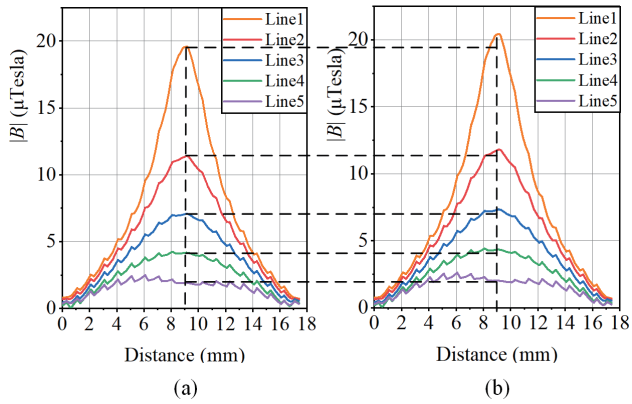

Fig. 4. Magnetic flux density along observation lines. (a) Gapped inductor, (b) Inductor with gap current sheets.

sheets in replacing the air-gap, Fig. 3 shows the 2-D FEM simulation results. The results reveal that the magnetic flux density distributions within the core windows of both inductors are essentially identical. To quantitatively assess the conformance of the flux density distributions, five green lines illustrated in Fig. 2 were used for flux density observation. The comparison of the flux density distributions along five observation lines of the two schemes is shown in Fig. 4, which demonstrates that the distributions exhibit remarkable consistency in both regularity and magnitude. Hence, the same eddy current will be induced in IUT because the distribution of eddy currents is determined by the flux density in the winding. Therefore, the winding losses in the two configurations are the same, validating the effectiveness of gap current sheets.

B. Replace the Air-Gap With WEAG

In Part A, the distribution of magnetic flux within the core window of the gapped inductor is the same as that in the gapless inductor through the application of gap current sheets. Therefore, the magnetic field equivalence within the core window of the gapped inductor can be realized by equating the magnetic potential drop of the air-gap.

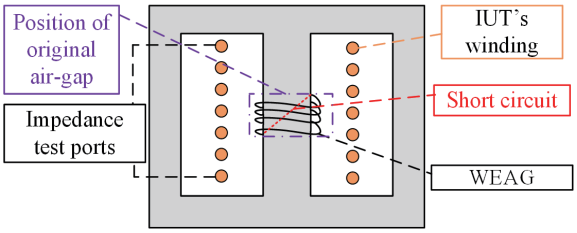

Fig. 5. Schematic diagram of winding short-circuit method with WEAG instead of air-gap.

In practical application, gap current sheets can be achieved by using short-circuited winding. Fig. 5 shows the measurement method of the winding loss in a gapped inductor, where the air-gap is replaced with a short-circuited winding. This winding is defined as the winding for equivalent air-gap (WEAG) in this article. It should be tightly wound around the original position of the air-gap on the center limb of the gapless core. The height of the winding should be the same as the original air-gap and its two terminals should be short-circuited. The WEAG and the winding of IUT constitute a transformer without an air-gap. Based on this, the transformer winding short-circuit method can be applied to the winding loss measurement of gapped inductors. It is worth mentioning that Fig. 5 shows a schematic that is just intended to show the structure of WEAG in a gapless inductor. To better illustrate its structure, the proportion of it is different from Fig. 2.

The loss measured from the input terminals of the gapped inductor contains both the winding loss and the core loss. Hence, it is important to eliminate the influence of core loss on the measurement results. A common method for calculating core loss is the Steinmetz equation:

$$P_{CV} = k \bullet f^{\alpha} \bullet B_m^{\beta} \tag{1}$$

where P_{CV} represents the core loss per unit volume, f denotes the frequency, and B_m means the peak magnetic flux density. k, α, and β are called Steinmetz coefficients, and they vary with material and temperature.

It can be learned from (1) that the core loss P_{CV} is closely related to the magnitude of the main-flux B_m. As observed in Fig. 3(a), a large amount of main-flux exists in the gapped inductor, which can cause core loss.

As depicted in Fig. 3(b), there is no main-flux inside the gapless inductor, excluding the region near gap current sheets. This is because the magnetizing magnetomotive force (MMF) is cancellated by gap current sheets instead of being used as a magnetic potential drop on the air-gap. Therefore, the air-gap equivalent scheme not only characterizes the magnetic field distribution in the core window of the gapped inductor but also largely eliminates the core loss of the inductor.

Since the main-flux in the core is negligible, the measured loss of the transformer in Fig. 5 is winding loss without

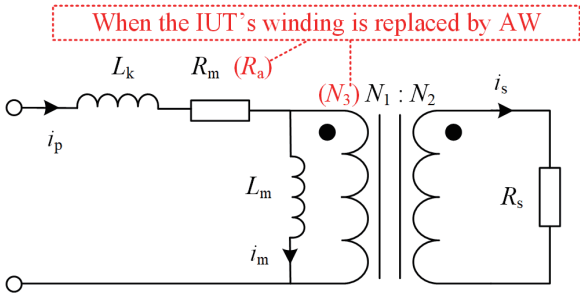

Fig. 6. Equivalent circuit model of transformer winding short-circuit method.

core loss. It is worth noting that core loss is determined by frequency and flux density, exhibiting a nonlinear relationship with current magnitude. Conversely, the relationship between winding loss and current magnitude is linear, which can be expressed as follows:

$$P_W = I^2 \bullet R_{AC} \tag{2}$$

Thus, the AC resistance obtained under the small-signal impedance test can accurately estimate the winding loss. Furthermore, under the condition of ampere-turns balance, the small-signal impedance test can significantly minimize the impact of core loss on the measurement results.

Fig. 6 shows the equivalent circuit model of the transformer winding short-circuit method. The same as the definition in Section I, R_m is the resistance of the IUT's winding, R_s is the resistance of WEAG, and R_a is the resistance of auxiliary winding (AW, it will be introduced in Section III). Additionally, L_k is leakage inductance and L_m represents magnetizing inductance. As for i_p, i_m, and i_s, they are the currents on their corresponding branches. Furthermore, N_1, N_2, and N_3 correspond to the number of turns in the IUT's winding, WEAG, and auxiliary winding, respectively.

Based on the ampere-turn balance, the relationship between i_pN_1, i_mN_1 and i_sN_2 can be derived as:

$$i_pN_1 = i_mN_1 + i_sN_2 \tag{3}$$

where i_m can be expressed as:

$$i_m = \frac{i_sR_s\dfrac{N_1}{N_2}}{2\pi fL_m} \tag{4}$$

According to (4), when $2\pi fL_m$ is much larger than R_sN_1/N_2, i_m can be regarded as 0. Then, L_m branch can be considered an open circuit, so the resistance R_{test1} measured from the test ports meets the following relationship:

$$R_{test1} = R_m + R_s\left(\frac{N_1}{N_2}\right)^2 = R_m + R_s^* \tag{5}$$

where R_s^* is the equivalent resistance of R_s transformed to the primary side. Therefore, it is only necessary to subtract R_s^* from R_{test1} to obtain the value of R_m.

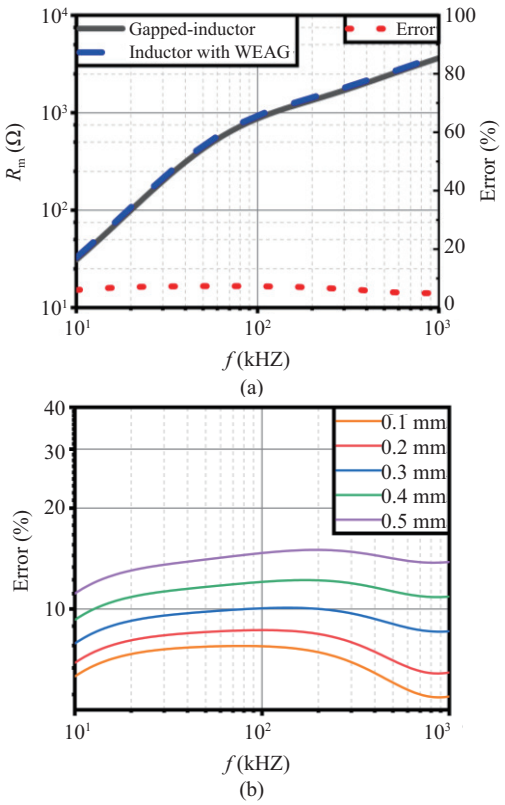

Fig. 7. R_m and errors varies with frequency in gapped inductor and inductor with WEAG. (a) WEAG attached to center limb, (b) the distance between WEAG and IUT's winding is changed.

Fig. 7 illustrates the FEM simulation results of the gapped inductor and inductor with WEAG, where the excitation current assigned in the simulation was 1 mA and the depth of the 2-D model was 1 m. As can be seen from Fig. 7(a), the R_m of the two inductors are almost identical within the frequency of 10 kHz to 1 MHz, with a maximum error of less than 7%. Therefore, the scheme of using a gapless inductor with WEAG to replace the gapped inductor for winding loss measurement is feasible. Fig. 7(b) shows the error of R_m after the distance between WEAG and IUT's winding was changed. WEAG was changed from 0.1 to 0.5 mm away from the center limb of the core. It can be seen that the closer WEAG is to IUT's winding, the greater the error. Therefore, in practical application, WEAG should be attached to the center limb as much as possible.

III. Resistance Separation of the IUT's Winding From WEAG

In Section II, a transformer was constructed using the winding of IUT and WEAG, and the AC resistance of the transformer winding was obtained under the impedance test. This scheme enables the separation of winding loss and core loss, but the measured resistance is the sum of R_m and R_s. In order to obtain R_m, it is necessary to remove R_s from the measurement results.

A. Take the DC Resistance as the AC Resistance of WEAG

Both the enameled wire and copper foil can be used as WEAG with the requirement that the wire gauge is as thin as possible, which can minimize the impact of skin effect on the AC resistance. Therefore, the DC resistance of WEAG can be regarded as the AC resistance at the low-frequency range, and the calculation of R_m is possible [20].

The reason why Litz-wire is not used is due to the reason that the twisting characteristic of it complicates the theoretical calculation of its DC resistance. The solid-round-wire with the small diameter is more suitable to be used as WEAG because its DC resistance is easy to obtain through the following formula:

$$R_{s\_DC} = \frac{\rho l N_2}{\pi\left(\frac{\delta}{2N_2}\right)^2} = \frac{4\rho l\left(N_2\right)^3}{\pi\delta^2} \tag{6}$$

where ρ is the conductivity of copper, l is the winding length of one turn, and δ is the height of the air-gap.

Another method is using thin copper foil to fabricate WEAG. Typically, only one turn of copper foil is used, and its DC resistance can be derived from (7), where σ is the thickness of the copper foil.

$$R_{s\_DC} = \frac{\rho l}{\sigma\delta} \tag{7}$$

The advantage of using copper foil lies in the lower technological requirements for constructing WEAG. Nevertheless, due to its greater susceptibility to eddy current effects, the degree of AC resistance variation in copper foil is higher than that of Litz-wire and solid-round-wire.

B. Replace IUT's Winding With Auxiliary Winding

As the frequency increases, the proximity effect will result in a significant increase in the AC resistance of WEAG, even when the Litz-wire is used for its construction. Additionally, WEAG is placed in the region where the diffusion-flux is most intense. Both two factors can affect the AC resistance varying with frequency. Therefore, accurately obtaining the AC resistance of WEAG is crucial for extracting R_m from the measurement results.

Based on the equivalence of magnetic potential difference, the air-gap can be replaced with WEAG to achieve the desired magnetic potential drop. Hence, a comparable approach can be employed to generate the MMF of the IUT's winding. According to that, this paper proposes a method for substituting the IUT's winding with AW. A new transformer is constructed using AW and WEGA, and then the total AC resistance of the two is determined by the winding short-circuit method.

Since a new influencing factor is introduced, the AC resistance of AW (R_a) needs to be removed. The separation of R_a and R_s is easier than that of R_m and R_s. Due to WEAG being tasked with simulating the function of the air-gap, its setting requirements are more stringent. Conversely, the AW simulates the IUT's winding, offering greater flexibility and facilitating the deduction of its AC resistance. In constructing AW, the selection of its wire gauge and its position are crucial. A well-designed AW can minimize the impact of this substitution on the measurement results. The key points for the construction of AW are as follows:

1) Selection of wire gauge. To minimize the impact of AW on the measurement results, its resistance should be as small as possible. Simultaneously, its AC resistance should not be easily influenced by the fringing effect. Litz-wire is the most suitable choice owing to its inherent characteristics. Litz-wire is less susceptible to the interference of external magnetic fields and primarily impacted by internal proximity effects, facilitating the measurement of its AC resistance through an air-core inductor.
2) Position of AW. To ensure that AW effectively simulates the MMF of the IUT's winding, it is crucial to place it appropriately. This could involve aligning it with WEAG, positioning it slightly further away from or keeping some distance from it.

AW generates an equivalent magnetic potential drop in WEAG with that of the IUT's winding when the ampere-turn balance of (8) is achieved.

$$i_p N_1 = i_p' N_3 \tag{8}$$

AW is required to be configured with just one turn, to minimize its resistance and mitigate the impact of external magnetic flux on it. Therefore, for AW constructed with a single-turn Litz-wire, its AC resistance remains almost consistent regardless of whether the inductor is equipped with a magnetic core. This allows for the measurement of its AC resistance by using an air-core inductor. Additionally, if required, AW can be designed to move slightly away from the WEAG, thus enhancing the consistency of its resistance across inductors with or without core.

C. Finite Element Simulation

The 2-D finite element simulations were conducted on the inductors with WEAG, which were excited under the IUT's winding and the single-turn AW, respectively. The excitations assigned in the simulation meet (8) and the results are shown in Fig. 8. As depicted in Fig. 8(a) and Fig. 8(b), when the AW is aligned with WEAG, the magnetic flux density distribution within WEAG is closest to that excited by IUT's winding, and the main-flux in the core is almost zero. The main-flux in Fig. 8(c) is slightly larger than that in Fig. 8(b), indicating that a higher coupling coefficient between AW and WEAG results in a smaller error of magnetic field equivalence. In Fig. 8(d), a low degree of coupling between AW and WEAG leads to an incomplete cancellation of MMF, resulting in numerous main-flux generated near AW. Such winding configurations should be avoided in practical applications.

Fig. 9(a) demonstrates the R_s of schemes in Fig. 8. It is evident that the simulated R_s do not have much difference

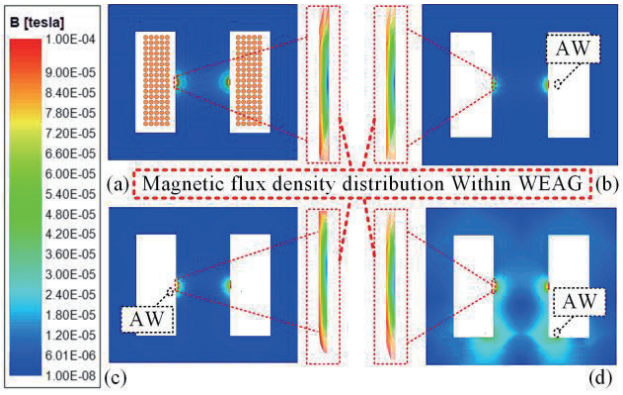

Fig. 8. Magnetic flux density distribution under different excitation windings. (a) IUT's winding, (b) AW scheme 1: aligned with WEAG, (c) AW scheme 2: Located 0.6 mm below WEAG, (d) AW scheme 3: at the bottom of the skeleton.

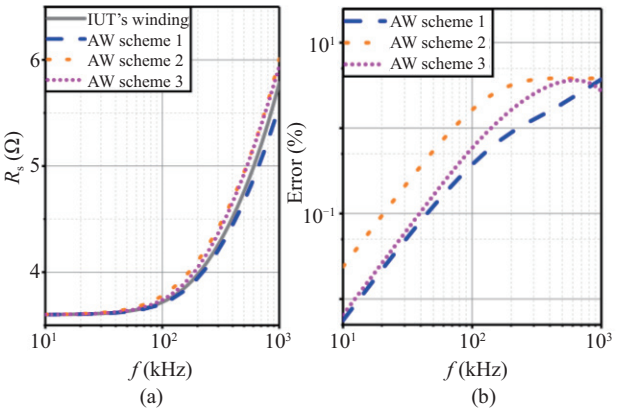

Fig. 9. R_s and errors vary with frequency. (a) R_s, (b) Errors.

across different excitation windings. In Fig. 9(b), the R_s excited by IUT's winding is taken as the benchmark, and the errors of the AW schemes compared against it are shown. The scheme that AW aligned with WEAG exhibits the least error. Notably, the errors of AW Scheme 1 and AW Scheme 2 have little difference. Therefore, in practical applications, considering the impact of diffusion-flux on AW, it is advisable to place AW slightly away from WEAG to mitigate the influence of the fringing effect on the AC resistance of AW.

D. Measure the AC Resistance of WEAG

Based on the analysis in parts B and C, AW can be used to generate the equivalent MMF instead of that generated by IUT's winding, thus obtaining the AC resistance of WEAG. This approach is straightforward and convenient for practical applications. A transformer composed of AW and the gapless core with WEAG should be fabricated, and AW needs to be located on the same skeleton as IUT. The total resistance R_{test2} can be measured using the short-circuit method as Fig. 6, and R_{test2} can be expressed as:

$$R_{test2} = R_a + R_s\left(\frac{N_3}{N_2}\right)^2 \tag{9}$$

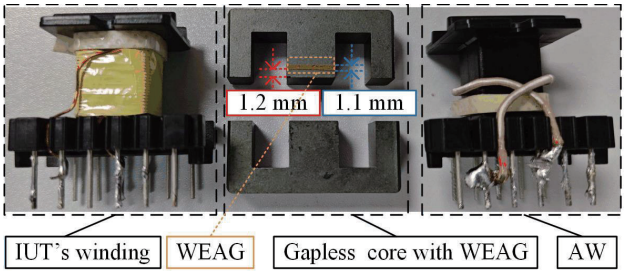

Fig. 10. Magnetic components made of EE35 core for measurements.

where R_a is the resistance of AW crafted from a single-turn Litz-wire. The resistance of Litz-wire is sufficiently small, and its AC resistance is barely influenced by the external magnetic field. The proximity effect among the individual strands of Litz-wire is the primary determinant of its AC resistance. Therefore, R_a can be measured using an air-core inductor, and then R_s can be extracted from (9).

By combining (5) and (9), an expression for R_m calculation based on the proposed method can be obtained:

$$\begin{aligned} R_m &= R_{test1} - R_s\left(\frac{N_1}{N_2}\right)^2 \\ &= R_{test1} - \left(\frac{N_1}{N_2}\right)^2 \left(R_{test2} - R_a\right)\left(\frac{N_2}{N_3}\right)^2 \\ &= R_{test1} - \left(\frac{N_1}{N_3}\right)^2 \left(R_{test2} - R_a\right) \end{aligned} \tag{10}$$

All variables in (10) can be obtained from measurements. Compared to the method of using DC resistance as a substitution for AC resistance, this approach reduces the impact of frequency changes on R_s. Thus, the error of R_s to measurement results is reduced in a wide frequency range, offering higher practicality.

IV. Experimental Verification

To validate the effectiveness of the proposed method, the magnetic components made of EE35 cores as shown in Fig. 10 were created for impedance measurement. The measurement results were compared with the simulation results of the 3-D eddy current field. In order to guarantee the consistency between the 3-D simulation models and the actual inductors, single-layer winding structure was adopted. Detailed parameters are listed in Table I.

Fig. 11 shows the test platform for impedance measurement, where the device employed is LCR-8110G produced by GWINSTEK. Fig. 12 illustrates the 3-D simulation models of the gapped inductor and the inductor with WEAG. To save computing resources, 1/4 models were adopted.

Fig. 13 shows R_m obtained from different approaches:

1) FEM-scheme 1: simulated gapped inductor;
2) FEM-scheme 2: simulated inductor with WEAG;
3) Scheme in [20]: measured AC resistance deducts the

TABLE I
PARAMETERS OF IUT MADE OF DIFFERENT CORES

Core type		EE35	EE28	EE16	RM10	PQ 2020
Air-gap	Height/mm	1.1	1.6	1.0	1.55	0.80
	d/mm	1.2	0	0.3	0.30	0.05
IUT's winding	Number of turns	22.0	16.0	13.0	15.00	12.00
	Diameter/mm	0.5	0.6	0.6	0.60	0.60
WEAG		Single-turn winding using a thickness of 0.065 mm copper foil.				
AW		Single-turn winding using 100 strands of Litz-wire, the diameter of each strand is 0.1 mm. Wound tight to a skeleton in the position 1 mm below WEAG.				

d: Distance from lowest point of WEAG to midpoint of the center limb.

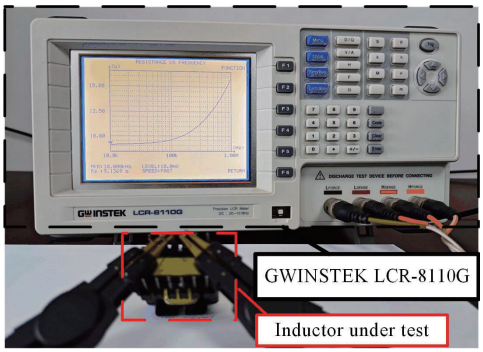

Fig. 11. Test platform for AC resistances.

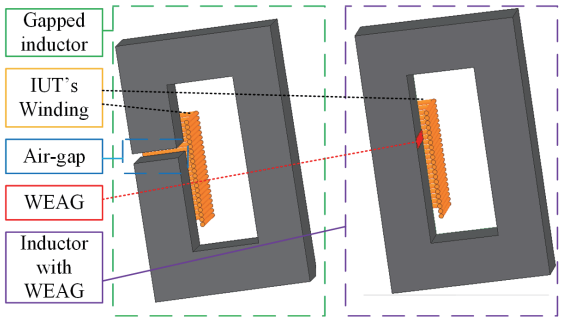

Fig. 12. 1/4 models of inductors for 3-D simulation.

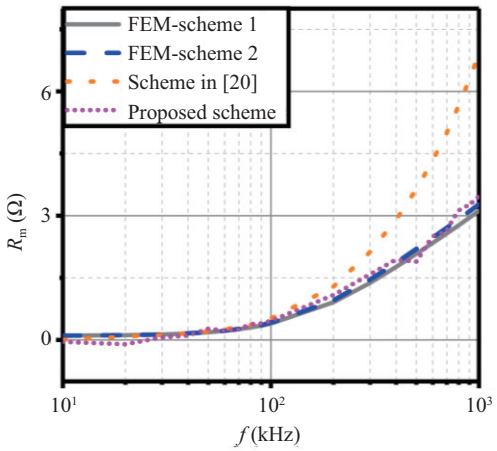

Fig. 13. R_m obtained from different approaches.

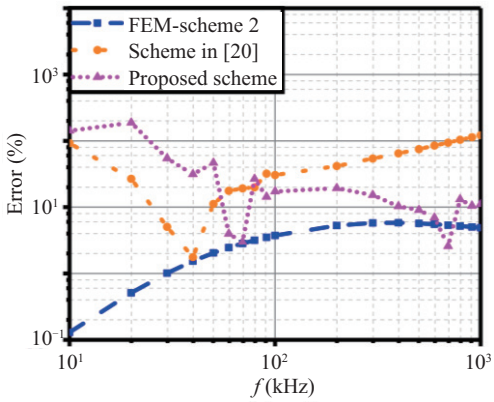

Fig. 14. Errors between other schemes and FEM scheme 1.

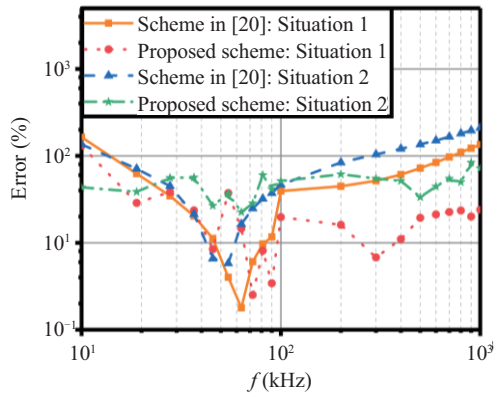

Fig. 15. Errors of schemes when changing the distance between WEAG and IUT's winding.

calculated DC resistance of WEAG;

4) Proposed scheme: measured AC resistance deducts the measured AC resistance of WEAG.

Fig. 14 demonstrates the errors between other schemes and FEM-scheme 1. It can be seen that the error of FEM-scheme 2 increases with frequency in the range of 10 kHz to 1 MHz, yet it consistently remains within 10%.

Scheme in [20] exhibited errors exceeding 20% at frequencies below 22 kHz. This is because when the frequency is low, the impedance of the magnetizing inductance is not large enough and its branch cannot be regarded as an open circuit. Consequently, employing (5) to calculate R_m introduces significant inaccuracies. Within the range of 22 to 80 kHz, the error was less than 20%. However, as the frequency rises the AC resistance of WEAG increases significantly to far larger than its DC resistance, leading to escalating measurement errors. Hence, the scheme has a limited frequency application range.

The proposed scheme also exhibited considerable errors at frequencies below 53 kHz, which is also attributed to the insufficient impedance of the magnetizing inductance in the process of using the short-circuit method twice. Nevertheless, the scheme had enough accuracy at higher frequencies. Specifically, the error remained within 20% from 53 to 400 kHz and droped to 10% at the range of 400 kHz to 1 MHz.

Fig. 15 shows the error of the proposed scheme for changing

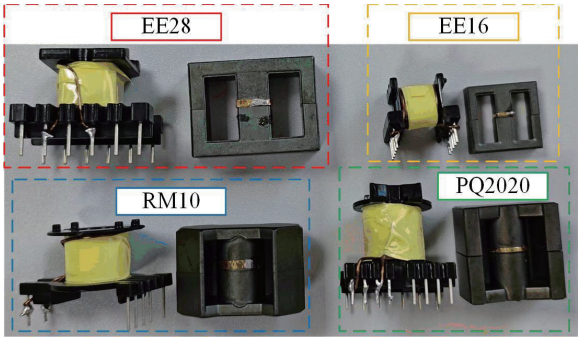

Fig. 16. Different sizes and different structures of inductors under test.

the distance between WEAG and IUT's winding by adding tape between WEAG and the center limb. Situation 1 is one layer and situation 2 refers to two layers of tape added, whose thickness is 0.2 mm. It can be seen that when only one layer of tape was added, the error of the proposed scheme could still be maintained at less than 20% after 60 kHz. In this situation, the scheme in [20] achieved the same effect only in the range of 37 to 95 kHz. After adding two layers of tape, both schemes became invalid with errors of more than 50% in most of the tested frequencies. But it is worth mentioning that in the two situations, the proposed scheme still had higher accuracy from 100 kHz to 1 MHz than the scheme in [20].

To further validate the method's robustness and applicability, the proposed scheme was applied to inductors with cores of different sizes and different structures. Fig. 16 shows the inductors under test and the results are demonstrated in Fig. 17. Detailed parameters of them are listed in Table I. The measurement errors came from comparisons between the two schemes and the 3-D FEM simulation results.

Fig. 17(a) shows the measurement results when the inductor was made of EE28 core. It can be found that from 230 kHz to 1 MHz, the proposed scheme had smaller errors than the scheme in [20]. Besides, the errors of the proposed scheme remained below 20% in the range of 86 kHz to 1 MHz. When the inductor was made from the EE16 core, the error of the proposed scheme was less than 20% from 220 kHz to 1 MHz as exhibited in Fig. 17(b). It's also in this range that the proposed scheme showed better results than the other.

Fig. 17(c) demonstrates the results when the inductor was made of RM10 core. The proposed scheme exhibited superiority over the scheme in [20] from 85 kHz to 1 MHz. The error of the proposed scheme remained below 15% in this range. When the inductor was with the PQ2020 core, as depicted in Fig. 17(d), the two schemes had similar accuracy before 100 kHz. However, the accuracy of the proposed scheme was higher than the scheme in [20] in the range from 150 kHz to 1 MHz.

As illustrated in Fig. 13 and Fig. 17, R_m has a steep growth tendency after 100 kHz, emphasizing the importance of accurately measuring the AC resistance of WEAG in the high-frequency range. Hence, the proposed scheme is particularly suitable for evaluating the winding loss of gapped inductors operating at high switching frequencies.

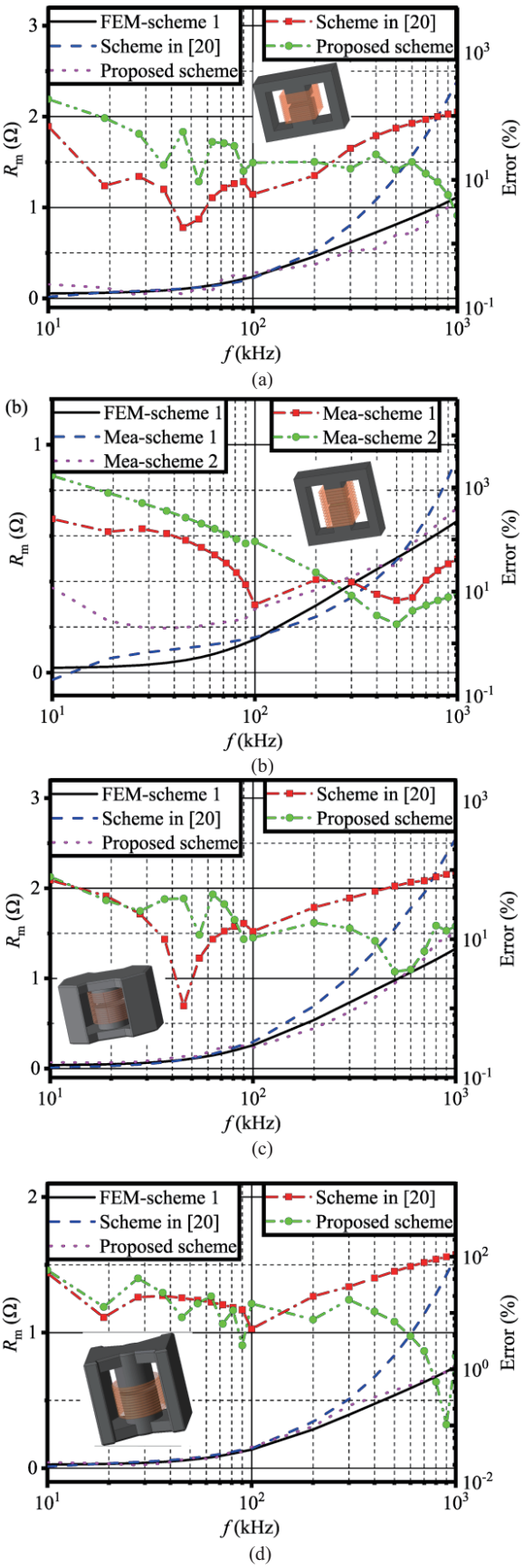

Fig. 17. Errors of the proposed scheme applied to inductors with different cores. (a) EE28, (b) EE16, (c) RM10, (d) PQ2020.

V. Error Analysis

The analysis and experiments conducted in the previous sections demonstrate the feasibility of the proposed method. However, as a measurement technique, it is imperative to perform an error analysis. The errors of the proposed method are categorized into the following types:

1) Error in replacing the air-gap with WEAG. Both the 2-D simulation in Section II and the 3-D simulation in Section IV indicate that this error maintains within 10%, which is reasonable.
2) Error of substituting AW for IUT's winding to generate MMF. The 2-D finite element simulation of different AW schemes in Section III shows that the AC resistance error of WEAG is within 10%, which is acceptable.
3) Error caused by the core loss. Although the magnetic flux in the core is canceled by ampere-turn balance, a small portion of the main-flux still exists near WEAG. This introduces an error due to core loss in the measurement results. However, since the winding loss is indirectly obtained by measuring the AC resistance under the small signal, the core loss is further reduced, making this error negligible.
4) Error introduced by the transformer winding short-circuit method. In the process of using this method, the branch of magnetizing inductance is treated as an open circuit. However, this requires that the impedance of magnetizing inductance is much greater than that of the secondary winding transformed to the primary side. Therefore, this method may introduce significant errors at low frequency. Since the proposed scheme uses the method twice, the error is large in the low-frequency range. However, at low frequencies, the change in the AC resistance of R_m compared to its DC resistance is very small, so the AC resistance can be equal to the DC resistance.
5) Error caused by using an air-core inductor to measure R_a. The key to reducing this error lies in the wire gauge selection and position of AW. By minimizing the resistance of AW and choosing an appropriate winding position, this error can be reduced to a reasonable range.

VI. Conclusion

This paper proposes a method for measuring the winding loss in gapped inductors. By magnetic field equivalence twice, this method obtains the total resistance of R_m and R_s, as well as the total resistance of R_a and R_s. After measuring R_a using an air-core inductor, the transformer winding short-circuit method is used to extract R_m. Through finite element simulation and experimental verification, the following conclusions can be drawn:

1) The use of a gapless inductor with WEAG to characterize the magnetic field of the gapped inductor is feasible, with an error of less than 10%.
2) AW can substitute IUT's winding for generating MMF, effectively characterizing the magnetic field of WEAG excited by IUT's winding. The margin of error across various AW configurations remained within 10%.
3) Impedance test demonstrated that this method has sufficient measurement accuracy in the high-frequency range. By applying the proposed method to inductors with cores of different sizes and structures, the robustness and applicability of it were verified.

The proposed scheme is currently only applicable to inductors with a single air-gap, and future research will focus on its application in magnetic components with multiple air-gaps.

References

[1] Z. Li, W. Han, Z. Xin, Q. Liu, J. Chen, and P. C. Loh, "A review of magnetic core materials, core loss modeling and measurements in high-power high-frequency transformers," in *CPSS Transactions on Power Electronics and Applications*, vol. 7, no. 4, pp. 359–373, Dec. 2022.

[2] D. Neumayr, D. Bortis, J. W. Kolar, S. Hoffmann, and E. Hoene, "Origin and quantification of increased core loss in MnZn ferrite plates of a multi-gap inductor," in *CPSS Transactions on Power Electronics and Applications*, vol. 4, no. 1, pp. 72–93, Mar. 2019.

[3] Y. Tian, Y. Li, and J. Liu, "Fringing field analytical calculation of high frequency planar magnetic components," in *CPSS Transactions on Power Electronics and Applications*, vol. 7, no. 3, pp. 251–258, Sep. 2022.

[4] R. S. Kasikowski and B. Wiecek, "Fringing-effect losses in inductors by thermal modeling and thermographic measurements," in *IEEE Transactions on Power Electronics*, vol. 36, no. 9, pp. 9772–9786, Sept. 2021.

[5] T. Ewald and J. Biela, "Analytical winding loss and inductance models for gapped inductors with litz or solid wires," in *IEEE Transactions on Power Electronics*, vol. 37, no. 12, pp. 15127–15139, Dec. 2022.

[6] T. Ewald and J. Biela, "Frequency-dependent inductance and winding loss model for gapped foil inductors," in *IEEE Transactions on Power Electronics*, vol. 37, no. 10, pp. 12370–12379, Oct. 2022.

[7] J. Gyselinck and P. Dular, "Frequency-domain homogenization of bundles of wires in 2-D magnetodynamic FE calculations," in *IEEE Transactions on Magnetics*, vol. 41, no. 5, pp. 1416–1419, May 2005.

[8] D. Lin, C. Lu, N. Chen, and P. Zhou, "An efficient method for litz-wire AC loss computation in transient finite element analysis," in *IEEE Transactions on Magnetics*, vol. 58, no. 5, pp. 1–10, May 2022.

[9] S. Ehrlich, H. Rossmanith, M. Sauer, C. Joffe, and M. März, "Fast numerical power loss calculation for high-frequency litz wires," in *IEEE Transactions on Power Electronics*, vol. 36, no. 2, pp. 2018–2032, Feb. 2021.

[10] J. Lyu, H. C. Chen, Y. Zhang, Y. Du, and Q. S. Cheng, "Litz wire and uninsulated twisted wire assessment using a multilevel PEEC method," in *IEEE Transactions on Power Electronics*, vol. 37, no. 2, pp. 2372–2381, Feb. 2022.

[11] A. Rosskopf and C. Brunner, "Enhancing litz wire power loss calculations by combining a sparse strand element equivalent circuit method with a voronoi-based Geometry model," in *IEEE Transactions on Power Electronics*, vol. 37, no. 9, pp. 11450–11456, Sept. 2022.

[12] C. Peng, G. Chen, B. Wang, and J. Song, "Semi-analytical AC resistance prediction model for litz wire winding in high-frequency transformer," in *IEEE Transactions on Power Electronics*, vol. 38, no. 10, pp. 12730–12742, Oct. 2023.

[13] F. Grecki and U. Drofenik, "Calorimetric medium frequency loss measurement of the foil inductor winding," in *2021 IEEE 19th International Power Electronics and Motion Control Conference (PEMC)*, Gliwice, Poland, 2021, pp. 611–614.

[14] N. Rasekh, J. Wang, and X. Yuan, "A novel in-situ measurement method of high-frequency winding loss in cored inductors with immunity against phase discrepancy error," in *IEEE Open Journal of the Industrial Electronics Society*, vol. 2, pp. 545–555, 2021.

[15] B. X. Foo, A. L. F. Stein, and C. R. Sullivan, "A step-by-step guide to extracting winding resistance from an impedance measurement," in *2017 IEEE Applied Power Electronics Conference and Exposition (APEC)*, Tampa, FL, USA, 2017, pp. 861–867.

[16] K. Niyomsatian, J. J. C. Gyselinck, and R. V. Sabariego, "Experimental

extraction of winding resistance in litz-wire transformers—influence of winding mutual resistance," in *IEEE Transactions on Power Electronics*, vol. 34, no. 7, pp. 6736–6746, Jul. 2019.

[17] E. L. Barrios, D. Elizondo, A. Ursúa, and P. Sanchis, "Winding resistance measurement in power inductors - Understanding the impact of the winding mutual resistance," in *IEEE Access*, vol. 9, pp. 92224–92238, 2021.

[18] D. Hou, M. Mu, F. C. Lee, and Q. Li, "High-frequency core loss measurement method with partial cancellation concept," in *IEEE Transactions on Power Electronics*, vol. 32, no. 4, pp. 2987–2994, Apr. 2017.

[19] F. N. Javidi and M. Nymand, "A new method for measuring winding AC resistance of high-efficiency power inductors," in *IEEE Transactions on Power Electronics*, vol. 33, no. 12, pp. 10736–10747, Dec. 2018.

[20] J. Ye and W. Chen, "A novel evaluation and test method for gapped magnetics high-frequency winding losses," in *Proceedings of the CSEE*, vol. 35, no 7, pp. 1749–1755. Feb. 2015.

[21] W. Chen, X. Huang, and J. Zheng, "Improved winding loss theoratical calculation of magnetic component with air-gap," in *Proceedings of The 7th International Power Electronics and Motion Control Conference*, Harbin, China, 2012, pp. 471–475.

Zhiyong Qiu was born in Nanping, China, in 1998. He is working toward an M.S. degree in School of Electrical Engineering and Automation, Xiamen University of Technology. His research interest is electromagnetic interference in power converters.

Kaining Fu was born in Xiamen, China, in 1993. He received his M.S. and Ph.D. degrees from Fuzhou University, Fuzhou, China, in 2018 and 2021, respectively. He is presently working as a lecturer in the School of Electrical Engineering and Automation, Xiamen University of Technology. His current research interests include power conversion, high-frequency magnetics, EMI debugging and solutions, and electromagnetic field analysis and applications.

Wei Chen was born in Fuzhou, China. He received his M.S. and Ph.D. degrees at Fuzhou University in 1987 and 1990, respectively. He worked as a Senior Visiting Professor at CPES of Virginia Tech, Virginia, the USA, from 1996 to 1998. He had been with Delta Electronics Co., Ltd., as R&D Manager in Delta Power Electronics Center of Shanghai from 1999 to 2008. He has published more than 80 technical papers, including *IEEE Transactions and Proceedings*. He held more than 40 approved patents from China and the USA. His research interests include power conversion, high-frequency magnetic technology, EMI debug and solution, wireless power transfer, electromagnetic field analysis, and applications, etc.